

We are IntechOpen, the world's leading publisher of Open Access books Built by scientists, for scientists

6,900

Open access books available

186,000

International authors and editors

200M

Downloads

Our authors are among the

154

Countries delivered to

TOP 1%

most cited scientists

12.2%

Contributors from top 500 universities



WEB OF SCIENCE™

Selection of our books indexed in the Book Citation Index
in Web of Science™ Core Collection (BKCI)

Interested in publishing with us?
Contact book.department@intechopen.com

Numbers displayed above are based on latest data collected.
For more information visit www.intechopen.com



Laser-Induced Hydrodynamics in Water and Biotissues Nearby Optical Fiber Tip

V. I. Yusupov¹, V. M. Chudnovskii¹ and V. N. Bagratashvili²

¹*V.I. Il'ichev Pacific Oceanological Institute, Far Eastern Branch of Russian Academy of Sciences*

²*Institute of Laser and Information Technologies, Russian Academy of Sciences
Russia*

1. Introduction

This paper is aimed at revealing the mechanisms of therapeutic effects stimulated by a medium power (1–10 W) fiber laser induced hydrodynamics in water-saturated bio-tissues. Modern laser medical technologies widely employ delivery of laser light to irradiated tissues via optical fibers. Optical fiber easily penetrates through needle and endoscopic channels, and laser light can be delivered through a fiber for puncture and endoscopic operations. Several laser medical technologies (puncture multichannel laser decompression of disc, laser intervention upon osteochondrosis, surgical treatment of chronic osteomyelitis, endovenous laser ablation, etc.) are based on effective hydrodynamic processes in water-saturated bio-tissues. These hydrodynamic processes trigger cellular response and regenerative effects through the specific mechanisms of mechano-biology. In this work, we consider different kinds of effects stimulated by a medium power laser-induced hydrodynamics in the vicinity of a fiber tip surface, in particular, generation of vapor-gas bubbles, fiber tip degradation, and generation of intense acoustic waves. Presence of strongly absorbed agents (in a form of Ag nanoparticles, in particular) in laser irradiated water nearby optical fiber tip results in appearance of pronounced filamentary structures of these agents.

2. Therapeutic motivation

One of the modern tendencies in a low-invasive medical therapy is a medium power (1–10 W) laser treatment of connective tissues. The examples of such technologies are: laser engineering of cartilages (Bagratashvili et al., 2006); puncture multichannel laser decompression of disc (Sandler et al., 2002; Sandler et al., 2004); laser intervention upon osteochondrosis (Chudnovskii & Yusupov, 2008); laser treatment of chronic osteomyelitis (Privalov et al., 2001); endovenous laser ablation (Van den Bos et al., 2009); fractional photothermolysis (Rokhsar & Ciocon, 2009).

Treatment of osteochondrosis, for example, is based on laser-induced (0.97 μm in wavelength and 2–10 W in power) formation of multiple channels inside an intervertebral disc using silica fiber with a carbon coated fiber tip surface, in order to enhance laser light absorption nearby the fiber tip. Osteochondrosis is caused by such partial destruction of

intervertebral disc, followed by release of nucleus pulposus from disc in the form of hernia, which exerts pressure upon nervous roots thus giving pain. Fig 1a shows the scheme of formation of multiple laser channels inside intervertebral disc in the course of laser treatment of osteochondrosis (Sandler et al., 2002; Sandler et al., 2004; Chudnovskii & Yusupov, 2008). Transport laser delivery fiber passes inside the disc under treatment through a thin needle inserted to the disc (laser puncture procedure). Optical fiber is inserted through a thin needle via a posterolateral percutaneous approach under a local anesthesia. Important, that saline water is permanently introduced into the disc through the needle. Channel is formed by the heated fiber moving forward inside the disc. The fiber forms the channel and is shifted 1 -2 cm per 5 - 10 s inside the disc. Fig. 1b shows the example of such channels in nucleus pulposus of spinal disc formed by a fiber laser in the course of laboratory experiment (Sandler et al., 2004).

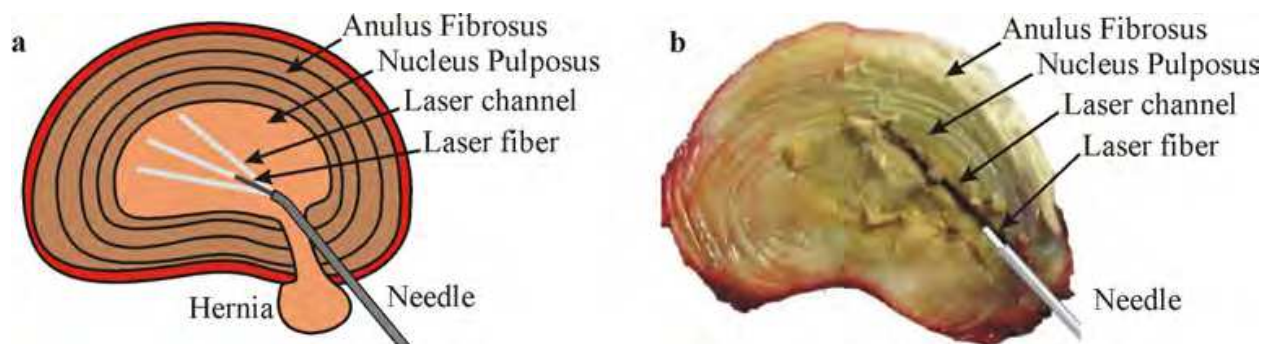


Fig. 1. a - Scheme of laser irradiation of spinal disc. b - Laser channel formed in spinal disc through optical fiber in presence of physiological solution (Sandler et al., 2004).

Surprisingly, that such action on herniated disc causes significant effect in some period of time on tissues located out of laser irradiated zone. As one can see, for example, on tomography picture (Fig. 2b), some cavities appear in the hernia, and its density decreases significantly compared with the density of hernia before laser treatment (Fig. 2a).

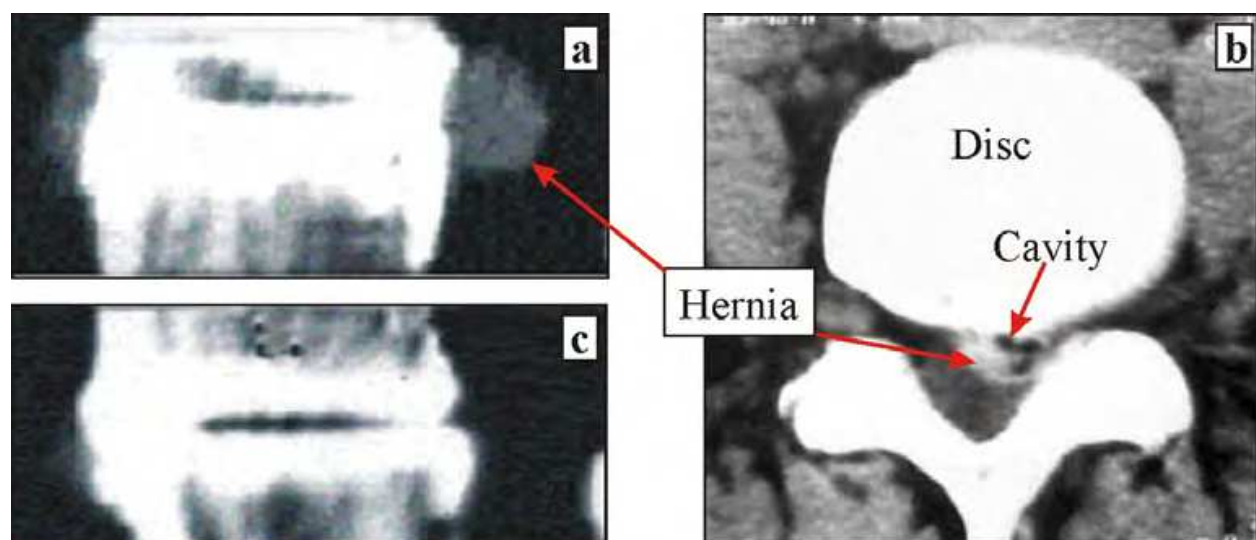


Fig. 2. Computer tomography pictures of herniated disc area. a- before healing: big sequester of hernia (side view); b - cavity inside hernia, stimulated by laser-induced channel formation in disc; c -three month after laser healing : no hernia.

As a result, the hernia transforms into a soft sponge, the pressure of hernia on nervous roots decreases, and relevant pain releases. The hernia itself disappears after some period of time, and regenerative processes take place which result (in a few month) in recovery of the disc structure and their main functions (Sandler et al., 2002, 2004; Chudnovskii et al., 2008, 2010a, 2010b).

Another important example of a medium power laser therapy is a laser treatment of chronic osteomyelitis. Fig. 3a demonstrates the X-ray image of femoral bone of the 14 year old patient heavily affected by osteomyelitis (Privalov et al., 2001). Significant destruction and rarefaction of bone structure takes place. Typically, such bone tissue degradation requires amputation of organ. However, application of medium power laser treatment approach in this case gave, as a result, a complete regeneration of affected femoral bone (Fig. 3b), and no amputation was required. Again, therapy was based on a medium power laser-induced formation of channels (similar to that presented at Fig.1) in a bone medullary tissue, which stimulate successively the regeneration processes in the bone tissue.

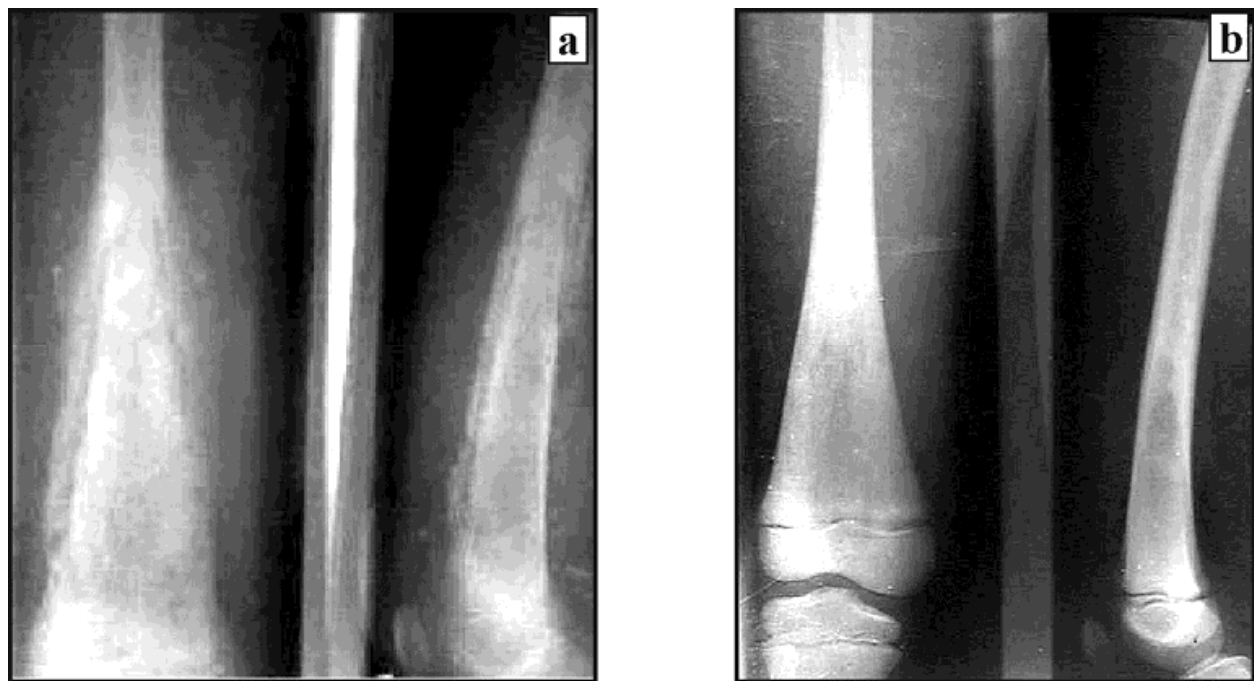


Fig. 3. X-ray images of right hip of the 14 y.o. patient with chronic osteomyelitis (Privalov et al., 2001). a - destruction and rarefaction of bone structure before treatment. b - complete regeneration of bone structure 11 month after laser treatment.

Strong regenerative potential of medium power laser treatment for different kinds of tissues is already well recognized (Sandler et al., 2002, 2004; Chudnovskii & Yusupov, 2008, Chudnovskii et al., 2010a, 2010b), however the dominant primary physical mechanisms of such regeneration are still the subject of controversy. It is commonly accepted that the effects of medium power laser irradiation result from laser heating of tissues. However in most of cases, the pronounced therapeutic effect cannot be rationalized by laser-induced thermal tissue degradation only. For example, appearance of cavities in the hernia and significant decrease of its density observed immediately after laser manipulation (Fig. 2b), takes place without its heating, since hernia is located quite far from the area of laser-induced channel formation, and, thus, heating of hernia is negligible.

We believe that *effective hydrodynamic processes* play dominant role for the effect of a medium power laser-induced regeneration and healing of connective tissues diseases (intervertebral hernia, osteomyelitis and some other diseases) using laser puncture procedures (Chudnovskii & Yusupov, 2008; Chudnovskii et al., 2010a, 2010b). Main features of these processes will be considered below.

3. Laser-induced generation of micro-bubbles in water

The key process for the mechanism of medium power laser-induced regeneration and healing of musculoskeletal system diseases is the generation of micro-bubbles in inter-tissue water (Yusupov et al., 2010).

3.1 Laser-induced generation of micro-bubbles in a free water

Formation of micro-bubbles in a free water was studied with the aid of the optical methods using a water filled plastic cell (the horizontal dimensions are 150×100 mm and the height is 15 mm) and glass capillaries with an inner diameter of 1 mm. In the most of experiments, the working fiber tip is preliminary blackened by a short (~ 1 s) contact of the fiber tip with a wooden plate at a laser power of about 3 W. The fiber tip surface thus covers by a thin carbon layer owing to the wood burning. Such a procedure is well reproduced, so that from 10 to 20% of the laser power is absorbed in the thin carbon layer. Computer controlled fiber lasers (LS-0.97 and LS-1.55 of IRE-Polus, Russia) with the wavelengths of $0.97 \mu\text{m}$ and $1.55 \mu\text{m}$, 1–10 W in power were interfaced with a $400 \mu\text{m}$ core diameter silica fiber. Low intensity (up to 1 mW) green pilot beam from the built in diode laser was used to highlight the laser irradiated zone in the cell. The fiber is horizontally fixed in the cell, which is placed on the worktable of a MICROS MC300 microscope equipped with a Vision digital color camera interfaced with PC. The water cell was also placed on the table with illumination, and the processes in the vicinity of the heated fiber tip were visualized using a Photron Fastcam SA-3 camera at rates of 2000 or 10000 frames per second. To control the laser induced spectrum, an Ocean Optics USB4000 fiber spectrum analyzer was used, which is interfaced with PC and has an optical resolution of about 1.5 nm and 200–1100 nm wavelength range. For better visualization of hydrodynamic flows the collargol (albumin coated Ag nanoparticles) have been added to water in the cell (Yusupov et al., 2011b).

Hydrodynamic flows taking place nearby the fiber tip when laser power is on, can be clearly seen in a scattering mode using illumination with green light of pilot laser beam through the same transport fiber (Fig. 4). Such flows result in intrusion of collargol from neighboring area into the area in front of the fiber tip. One can also see here the initial process of new intrusion formation (outlined with a dashed line). The rate of rise-up front of a given intrusion (which is about $150 \mu\text{m}$ in average thickness) is found to be described by exponential law (Yusupov et al., 2011b)

$$V = 0.6 \cdot \exp(-1.5 \cdot r), \quad (1)$$

where r is the distance from fiber tip: at 1 mm from fiber tip $V = 150 \mu\text{m/s}$, while at 2 mm from fiber tip V falls down to $30 \mu\text{m/s}$.

The bubbles don't occur up to laser power of 10 W with non-blackened fiber tip and for $0.97 \mu\text{m}$ laser radiation, while for $1.56 \mu\text{m}$ laser radiation (which is much stronger absorbed by water) the bubbles are generated at about 1 W of laser power. Blackening of fiber tip results in generation of bubbles for both $0.97 \mu\text{m}$ and $1.56 \mu\text{m}$ laser wavelengths.

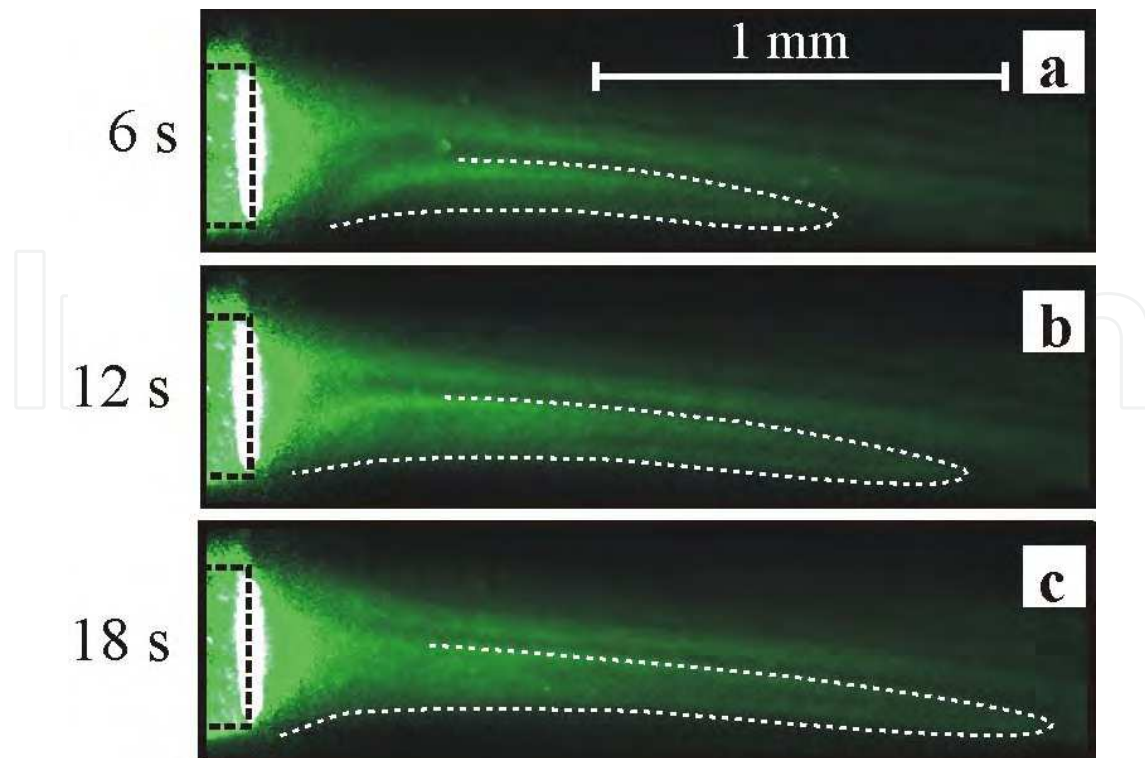


Fig. 4. Microscope pictures (in scattering mode) of intrusions of Ag nanoparticles in water (outlined with dashed line) stimulated by laser induced hydrodynamics nearby optical fiber tip at 1.0 W of 0.97 μm laser power in 6 s (a), 12 s (b), and 18 s (c) of laser irradiation. Fiber tip is shown by dashed line (Yusupov et al., 2011b).

Energy of incident laser light is partly (10–20%) absorbed by the carbon layer on the blackened fiber, so that the fiber is heated. When laser radiation with a power of greater than 3 W is transmitted by the fiber tip in air, the spectrum of the optical radiation from the fiber tip contains the fundamental line (0.97 μm or 1.56 μm) and the broadband visible and near-IR radiation caused by the heating of the tip surface to relatively high temperatures. When a blackened tip is placed into water, the tip surface is effectively cooled and the absence of the broadband radiation means the substantially lower temperatures of the tip surface. However, a medium power laser radiation (1–5 W) is sufficient for surface heating and generation of vapor-gas bubbles. When water is heated, the dissolved gases are liberated in the vicinity of the tip surface and gas bubbles emerge. Water is evaporated inside the bubbles, so that the bubbles are filled with vapor and, consequently, increase in size. At the lower boundary of the above power interval, the bubbles increase in size residing on the tip surface (Fig. 5a). When a critical size is reached, the bubbles are detached and move to the surface.

Water molecules which approach the heated tip surface acquire additional kinetic energy and momentum. The component of the total momentum of vapor molecules that is directed perpendicularly to the tip surface of the fiber towards water appears insufficient for the detachment of the bubble. Figure 5a shows that the bubbles sizes can be close to the diameter of the silica fiber core (400 μm). In the experiments, the bubbles normally emerge at same spots on a tip surface, which correspond to a high temperature areas. Evidently, the presence of such spots is related to the nonuniformity of the carbon layer: the absorbed energy (and, hence, the temperature) is greater for thicker regions. The stabilization (i.e., the

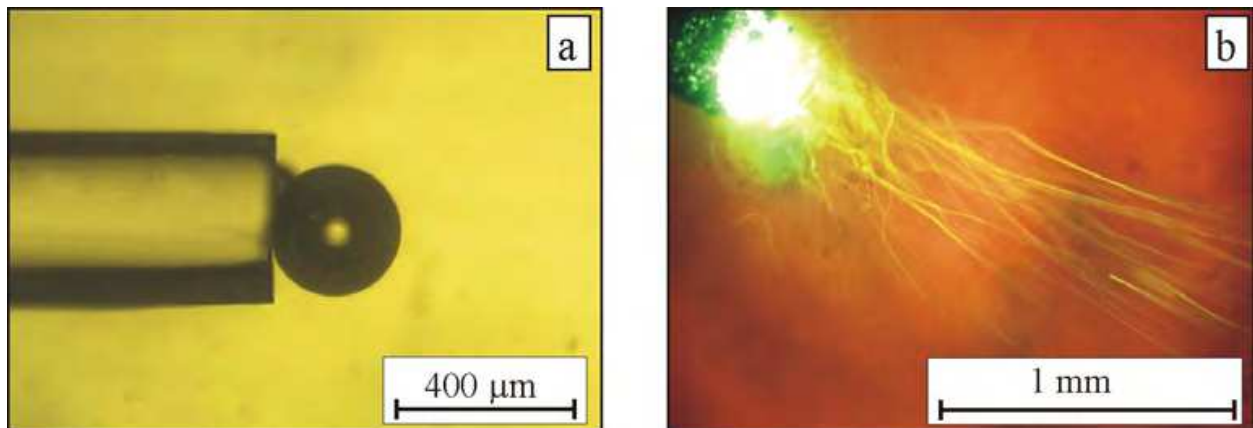


Fig. 5. Laser-induced generation of microbubbles in the vicinity of the blackened end surface of the optical fiber in water for the laser radiation with a wavelength of $0.97 \mu\text{m}$ and a power of (a) 1 and (b) 5 W. The photograph is taken from above at an exposure time of 250 ms.

attachment of the vapor-gas bubbles to the high temperature spots) can be caused by two reasons. First, the temperature at the hot spot additionally increases owing to the formation of the bubble and the consequent decrease in the local heat sink to water. The second reason is related to the Marangoni effect (Berry et al., 2000): the temperature gradient gives rise to the gradient of surface tension, so that convective flows emerge on the surface of the bubble and cause the force that presses the bubble to the hot spot. The experiments on the growth of the bubbles in the vicinity of the tip surface show that the rate of growth gradually decreases and, finally, the growth is terminated. At a laser power of 1 W, the duration of a relatively fast growth is about 200 ms. Bubble size increases at this stage from zero to 25% of the maximum size. Then, over a few seconds, the growth is well described with the formula (Yusupov et al, 2010):

$$D \propto t^{4/5}, \quad (2)$$

where D is the diameter of bubble and t is time. When laser light is terminated (Fig. 5a), the size of bubble gradually decreases (the bubble remains attached to the tip surface of the fiber) and, finally, the bubble vanishes. Note that a decrease in the size is also non-monotonic. At the first stage with a duration of less than 1 s, the diameter decreases by 8–10%. Then, the slowing takes place. Such a non-monotonic behavior must be related to the fact that the size of bubble decreases at the first stage predominantly, due to a decrease in the temperature of the vapor-gas mixture inside the bubble to the temperature of water in the cell, whereas the second stage is isothermal. The lifetime of such bubbles ranges from 3 to 8 h, and the rate of a decrease in the diameter with time always monotonically increases. At the second stage, the dependence of the diameter on time is well approximated with the formula (Yusupov et al., 2010):

$$D = D_0 \cdot (1 - t / \tau_0)^a, \quad (3)$$

where D_0 is the initial diameter, τ_0 is the lifetime, and $a = 0.1-0.5$ is the empirical parameter. Note a similar decrease in the diameter with time at $a = 0.5$ in (Taylor & Hnatovsky, 2004). A qualitatively different scenario corresponds to higher laser powers. The explosive boiling of water is observed in the vicinity of the hot end: the vapor-gas bubbles are ejected from the

fiber to water (Fig. 5b) and, then, the velocity decreases due to viscosity. At a finite exposure time the tracks of bubbles moving in water was observed. Notice that the track length corresponds to the mean velocity of the bubble over the exposure time. Bright spots in the vicinity of the tip surface (Fig. 5) are related to stray light: the Vision video camera is sensitive to the near-IR laser radiation.

The side measurements (Fig. 6a) show that the bubbles come to the surface at a certain distance from the fiber. Knowing the vertical velocity of the bubbles (about 5 mm/s in accordance with visual observations) and the trajectories, we can estimate the horizontal velocity (Fig. 6b). The analysis of the trajectories yields an exponential decrease in the horizontal velocity with increasing distance from the fiber: for the slowest and fastest bubbles, we obtain the dependences (Yusupov et al, 2010)

$$V = 67 \cdot \exp(-0,82 \cdot r) \quad (4)$$

and

$$V = 101 \cdot \exp(-0,74 \cdot r), \quad (5)$$

respectively, where V is the horizontal velocity in mm/s and r is the distance from the fiber tip surface in millimeters. The relationships show that the velocity of bubbles at the moment of the detachment from the fiber tip ($r = 0$) ranges from 67 to 101 mm/s.

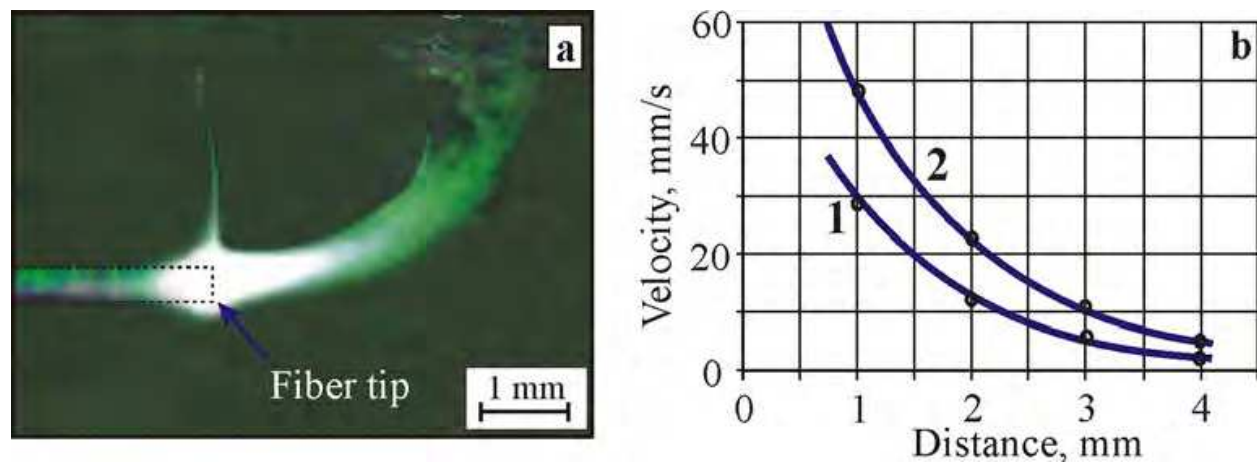
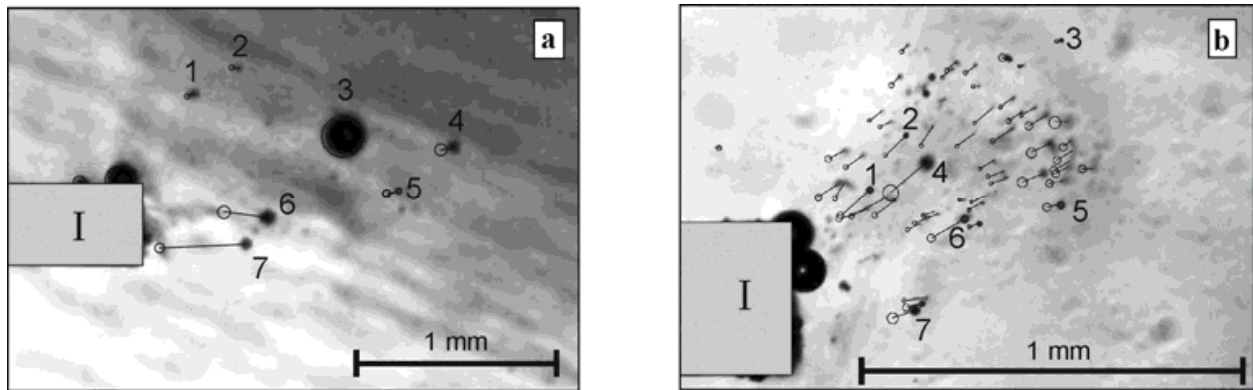


Fig. 6. a - Side view of the tracks of microbubbles in the vicinity of the blackened optical fiber tip surface in water; b - Plots of the horizontal velocity vs. distance from the end surface for slowest (1) and fastest (2) bubbles at a laser wavelength of $0.97 \mu\text{m}$ and a power of 5 W (Yusupov et al., 2010).

We have directly observed motion of bubbles even in the immediate vicinity of the surface tip (at the maximum velocities) in the experiments on the generation of microbubbles performed with the aid of the Photron Fastcam SA3. Fig. 7 shows the bubbles as dark circles with different sizes. Previous (at time step Δt) positions and sizes are shown as open circles, and the trajectories are shown as rectilinear segments. Table 1 presents the calculated sizes and velocities of the bubbles shown in Fig. 7. It is seen that the bubble with a diameter of $47 \mu\text{m}$ (bubble 7 in Fig. 7a and Table 1), which is initially located at a distance of about $100 \mu\text{m}$ from the fiber tip, moves at a mean velocity of 97 mm/s over the observation interval (4.4 ms).



Closed circles 1–7 show positions of bubbles, open circles show previous positions, and rectilinear segments show bubbles trajectories.

The images are taken from above at rates of (a) 10000 and (b) 2000 frames per second.

Laser powers of (a) 3 and (b) 6 W, time intervals $\Delta t =$ (a) 4.4 and (b) 2.0 ms, and a laser wavelength of 0.97 μm .

The pulse duration is 50 ms and the interval between pulses is 500 ms.

Fig. 7. Displacements of microbubbles (that are generated in the vicinity of the schematically shown blackened tip surface of quartz fiber I) over short time intervals Δt in the presence of laser radiation (Yusupov et al., 2010). **a** - CW laser radiation. **b** - Pulsed laser radiation.

Such result is in good agreement with the above estimations of the initial velocities in the vicinity of the fiber tip. The velocities of the bubbles rises rapidly with increasing distance from the fiber: the velocities are not higher than 50 and 20 mm/s at distances of 0.5 mm and 2 mm, respectively (Table 1). When bubbles are generated in a viscous liquid over a relatively long time interval the steady-state flow results in increase of the bubbles velocities. To determine the relative contribution of such a flow, we have measured the motion of microbubbles under the pulsed laser irradiation (Fig. 7b). It is seen that the bubbles predominantly move at relatively large angles relative to the fiber axis. That is caused by the features of the tip surface and hydrodynamic effects. Note that the asymmetry also corresponds to the motion of microbubbles under the continuous wave laser irradiation.

Number of the bubble (Fig. 7)	Parameters of radiation			
	CW radiation, 3 W (Fig. 7a)		pulsed radiation, 6W (Fig. 7b)	
	Diameter, μm	Velocity, mm/s	Diameter, μm	Velocity, mm/s
1	26	9	17	38
2	26	9	10	37
3	200	3	10	5
4	58	16	41	60
5	42	12	21	20
6	63	48	21	52
7	47	97	27	32

Table 1. Parameters of the bubbles shown at Fig. 7

Figure 7b and Table 1 show that a short laser pulse with power of 6 W causes generation of many bubbles, whose diameters range from 10 to 41 μm . The velocities of bubbles are 60 and 20 mm/s in the vicinity of the fiber and at a distance of 300 and 800 μm , respectively. In spite of a twofold increase in the laser power, the maximum velocities of the bubbles in the vicinity of the fiber under the pulsed irradiation are significantly less than the velocities corresponding to the continuous wave irradiation. At a relatively large distance from the fiber end, the velocities corresponding to the pulsed irradiation are also less than the velocities corresponding to the continuous wave irradiation: the velocity of bubble 4 in Fig. 7a is almost equal to the velocity of bubble 5 in Fig. 7b, whose distance from the fiber tip is almost two times shorter. Such result indicates to the presence of water flows in the case of the continuous wave laser irradiation and shows that the flow velocity is comparable with the mean velocity of bubbles.

Such liquid flows are more clearly observed in the microscopic measurements of the laser-induced hydrodynamic effects in the vicinity of the fiber tip surface of the fiber that is placed in a glass capillary filled with water.

3.2 Laser-induced generation of micro-bubbles in a glass capillary

Liquid flows are more clearly observed in the microscopic measurements of the laser-induced hydrodynamic effects in the vicinity of the fiber tip surface of the laser fiber that is placed in the glass capillary filled with water (model of the laser channel).

As it follows from Fig. 8, the attached vapor-gas bubbles at a laser power of 1–2 W emerge at the tip surface and the convective motion is observed in the liquid. A qualitatively different scenario corresponds to a power of 3 W: the microscopic bubbles ejected from the fiber tip move along arc shaped trajectories and entrain liquid flows (Fig. 8a). The intensity of the resulting vortices rapidly increases with increasing radiation power (Fig. 8b). In accordance with the estimations based on the frame-to-frame analysis of the video records, the period of the typical circulating liquid flows at laser powers of 3–5 W ranges from 0.2 to 1 s. Note that the above effects can be observed in the experiments with the blackened fiber tip at both laser wavelengths (0.97 μm and 1.55 μm). In the absence of the preliminary blackening, the effects are observed only for a radiation wavelength of 1.55 μm . Such a difference is caused by the fact that the radiation with a wavelength of 1.55 μm (unlike the short wavelength

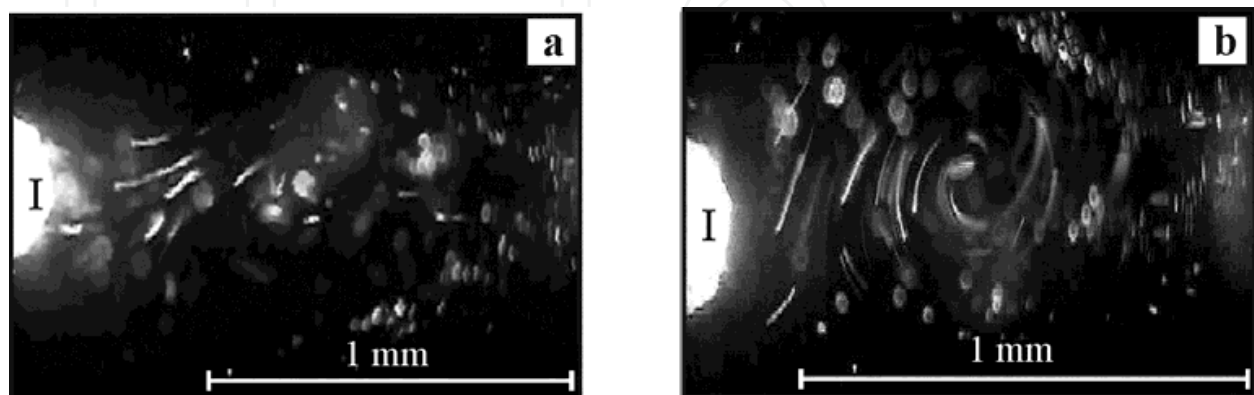


Fig. 8. Water flows that actively circulate inside the glass capillary (with a diameter of 1 mm) in the vicinity of the blackened tip surface I heated by the laser radiation with a wavelength of 0.97 μm and a power of 3 W (a) and 5 W (b)

radiation) is capable of heating a thin water layer in the vicinity of the tip surface to the boiling point, since the absorbance at a wavelength of $1.56 \mu\text{m}$ is higher than the that at a wavelength of $0.97 \mu\text{m}$ by a factor of about 20 (Hale & Querry, 1973).

It is possible to visualize the hydrodynamic flows occurring in capillary and caused by laser-induced bubbles generation by microscope visual observing the meniscus. To accomplish this, the silica optical fiber with a $400 \mu\text{m}$ diameter was introduced into a thin water-filled capillary with a $500 \mu\text{m}$ internal diameter. The volume of liquid in a capillary was about 20 mm^3 , and meniscus was located at a 25 mm distance from the fiber tip surface.

Fig. 9 demonstrates the observed variations of a meniscus shape in a glass capillary at a power of laser radiation of 1 W and at laser wavelength of $1.56 \mu\text{m}$. Switching of laser radiation on has resulted in growing the distance between optical fiber tip surface, which is caused by the fact that vapor-gas bubbles are formed in a liquid in the course of laser irradiation nearby a fiber tip. Simultaneously with a gradual rise of average volume of liquid in a capillary, quite a strong variations of meniscus shape takes place in this case, which are caused by hydrodynamic processes observing in a capillary water cell. At a certain period of laser irradiation time even water flows occur (Fig. 9b and 9c) caused, presumably, by the appearance and fast motion of quite large vapor-gas bubbles in a water capillary cell. Decrease of laser power causes increase of water streams, and in some cases the eruption of some portion of liquid from a capillary takes place.

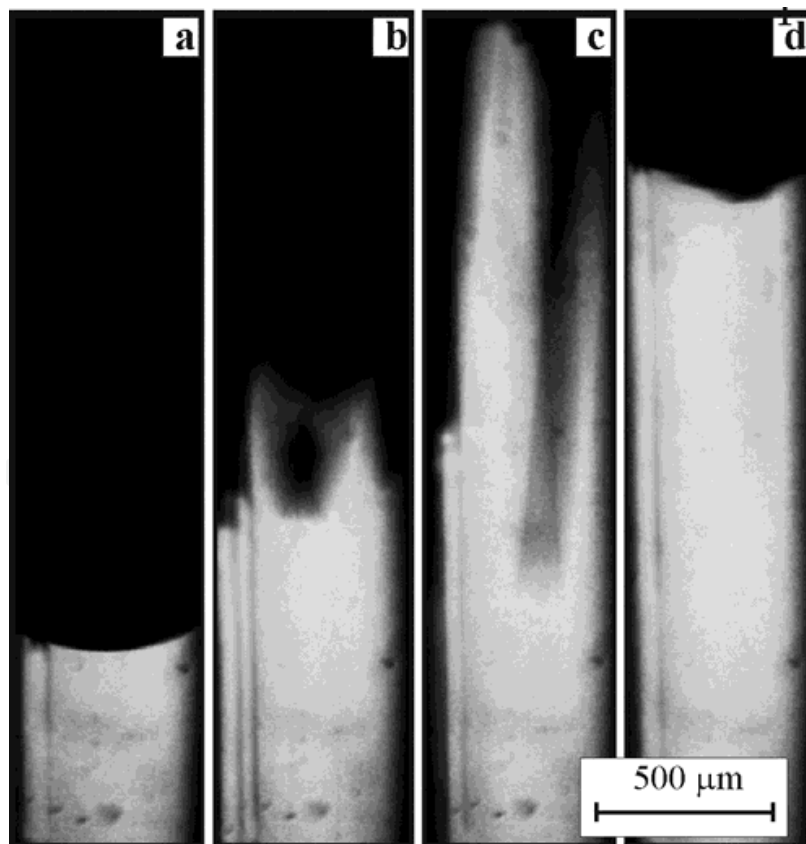
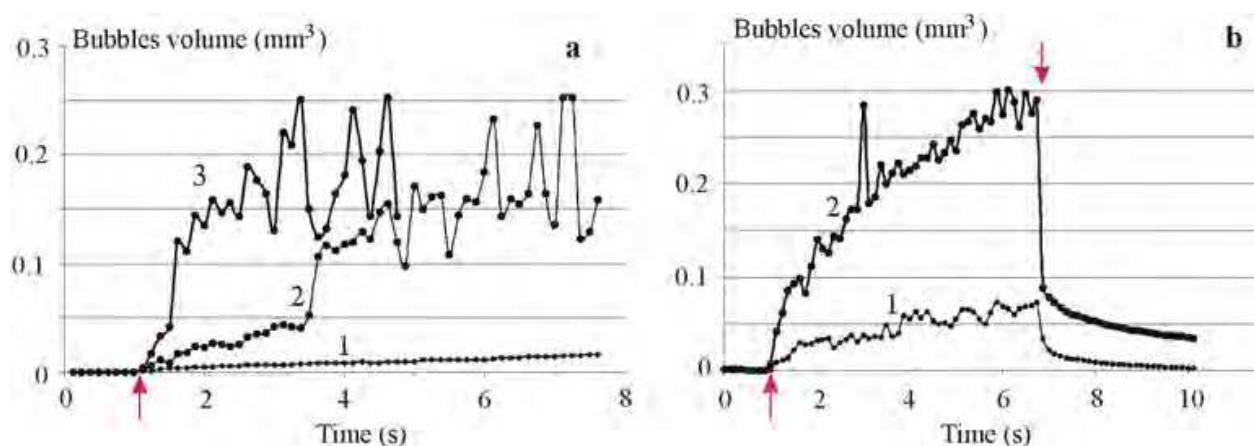


Fig. 9. Variation of a meniscus shape in a capillary caused by laser induce hydrodynamics and bubbles formation. Laser wavelength is $1.56 \mu\text{m}$, laser power – 1W , internal diameter of capillary - $500 \mu\text{m}$.

Knowing the level of the meniscus in a capillary it is possible to determine easily the total volume of vapor-gas bubbles. Fig.10 shows change in the volume of generated bubbles at different laser powers and different laser wavelengths. Our experiments show that the total volume of bubbles rises gradually with time by a logarithmic law after the laser radiation switching on. The total volume at 1 W of laser power rises with time monotonically for both wavelengths, while at higher laser power quite strong fluctuations take place, with the growing in time amplitude. As this takes place, at laser power of 3 W the strong eruption of liquid from the capillary was observed after 4.7 s of laser irradiation (curve 3 at Fig. 10a). At that moment the curve 3 interrupts, since the meniscus went out of visualization zone because of the abrupt decrease of meniscus level.

The total volume of generated bubbles increases with laser power. Comparison of curves 1 and 2 at Fig.10b shows that twofold increase of laser power (from 1 to 2 W) causes about the fourfold rise of the generated bubbles volume. After the laser radiation switching off, the total volume of bubbles first rapidly decreases (vapor condensation inside bubbles), and next decreases more slowly. It should be noted that quite a strong low-frequency oscillations are observed, caused by variation of total bubbles volume in a capillary.



In the case of $0.97\mu\text{m}$ wavelength the fiber tip surface was covered by a thin carbon layer.

Arrows show the moments of laser on and laser off.

Digits at curves shows laser power in Watts.

Fig. 10. Change of the total bubbles volume at different powers of lasers with $0.97\mu\text{m}$ (a) and $1.56\mu\text{m}$ (b) wavelengths of radiation.

Thus, the hydrodynamic processes related to the explosive boiling in the vicinity of the hot tip surface are observed in the liquid even at medium laser powers. Note that the intracapillary liquid exhibits effective mechanical oscillations with a frequency of 1–5 Hz and appears saturated with microbubbles. We expect the development of such laser-induced hydrodynamic processes in water-saturated biotissues at medium laser powers.

On the one hand, such processes provide the saturation of cavities and fractures in a spinal disc or bone with the water solution containing vapor-gas bubbles. On the other hand, they give rise to high-power acoustic oscillations and vibrations in the organ containing the connective tissue. Apparently, the filling of hernia with vapor-gas bubbles provides the reproducible decrease in the density of herniation immediately after the laser treatment (Sandler et al., 2004; Chudnovskii & Yusupov, 2008).

It is known from (Bagratashvili et al., 2006) that the mechanical action on cartilages in the hertz frequency range actively stimulates the synthesis of collagen and proteoglycans even at relatively small amplitudes. The above estimations show that the pressure on biotissue provided by the vapor-gas bubbles can reach tens of kilopascals. In accordance with (Buschmann et al., 1995; Millward-Sadler & Salter, 2004), such pressures in the hertz frequency range can lead to regenerative processes in cartilage owing to the activation of the interaction of the extracellular matrix with the mechanoreceptors of chondrocytes (integrins).

3.3 Laser-induced generation of bubbles microjets

Note an interesting phenomenon in the experiments on the generation of bubbles in the vicinity of the blackened tip surface of the fiber in the water cell: bubble microjets can be generated at a laser power of less than 3 W (Fig. 11) (Yusupov et al., 2010). The lengths of the microjets (Fig. 11a), which always start in the immediate vicinity of the fiber tip, reach several millimeters, the transverse sizes normally range from 10 to 50 μm , and the sizes of the bubbles that form the jets range from several to ten microns. The lifetime of the microjets ranges from a few fractions of a second to tens of seconds. A microjet that emerges at a certain spot on the tip surface remains attached to this spot and exhibits bending relative to the mean position. Bubble microjets didn't use to be continuous from start to end, the discontinuities used to appear on them, which used to restore quite often. The observations show (Yusupov et al., 2010) that the discontinuities are always related to the hydrodynamic perturbations and are caused by relatively large bubbles that move in the vicinity of the microjet. The appearance of quite a large bubble attached to the fiber tip caused the bubble microjet bending around large bubble (Fig. 11b). Thus, we conclude that two conditions must be satisfied for the generation of the bubble microjets. First, a hot spot must be formed on the tip surface. Second, the neighborhood of such a spot must be free of the centers that provide the generation and detachment of large bubbles. Note that the possibility of bubble microjets in the vicinity of a point heat source is demonstrated in (Taylor & Hnatovsky, 2004).

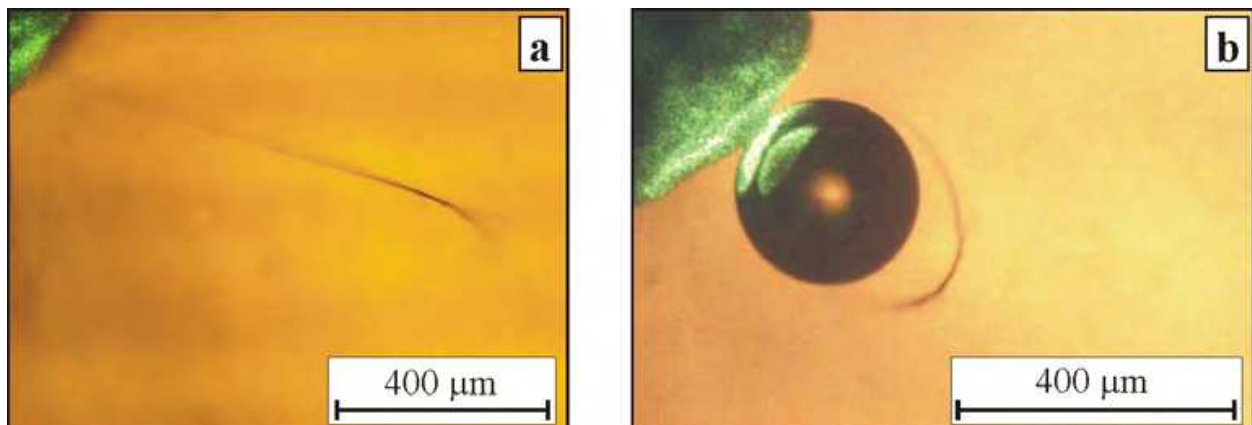


Fig. 11. Bubble microjets in the vicinity of the tip surface of optical fiber.

A part of the blackened fiber tip is shown at the right upper corner.

4. Degradation of optical fiber tip

Laser-induced hydrodynamic effects in water and bio-tissues can lead to the significant degradation of the fiber tip (Yusupov et al., 2011a). The most significant degradation of the

fiber tip surface occurs in the regime of channel formation when the fiber is shifted inside the wooden bar that mimics the biotissue. In this case, we observe substantial modifications and distortion of tip surface. The comparison of the sequential photographs (Fig. 12) shows a significant increase in the volume of the fiber fragment (swelling) in the vicinity of fiber tip.

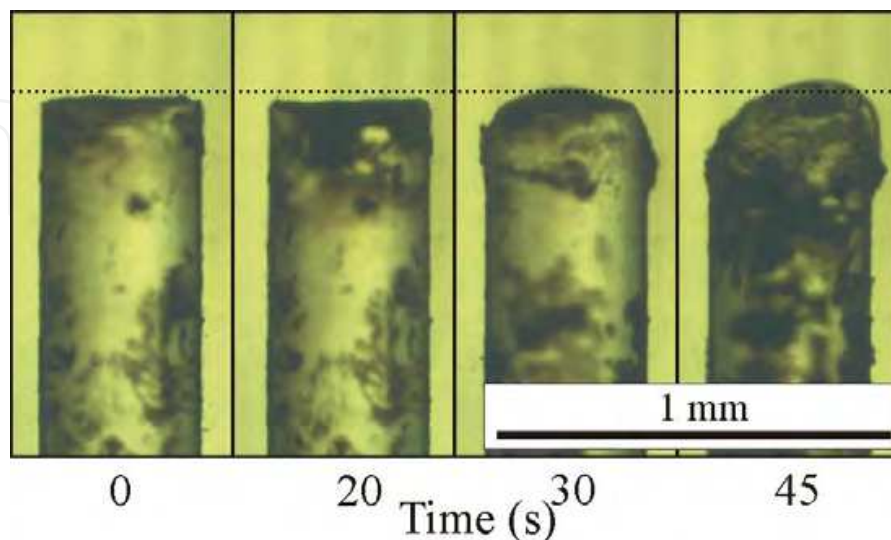


Fig. 12. Modifications of the profile of the blackened fiber tip surface (side view) for regime of channel formation (the channel is formed by the fiber that moves inside the wooden bar with water and the radiation power is 5 W). The left-hand panel shows the original fiber just after its blackening (Yusupov et al., 2011a).

SEM images (Fig. 13) show that the laser action in the regime of the channel formation in the presence of water causes substantial modifications of the working surface: the sharp edge is rounded and surface irregularities (craters) emerge on the tip surface. The image shows that a thin shell (film) with circular holes is formed at the tip surface of the optical fiber. Multiple cracks pass through some of the holes. In addition, we observe elongated crystal-like structures on the surface (Fig. 13b). Looking through the largest hole in the film on the tip surface (at the center of the lower part of the fragment at Fig. 13a), whose dimension in any direction is greater than $10\ \mu\text{m}$, we observe the inner micron-scale porous structure.

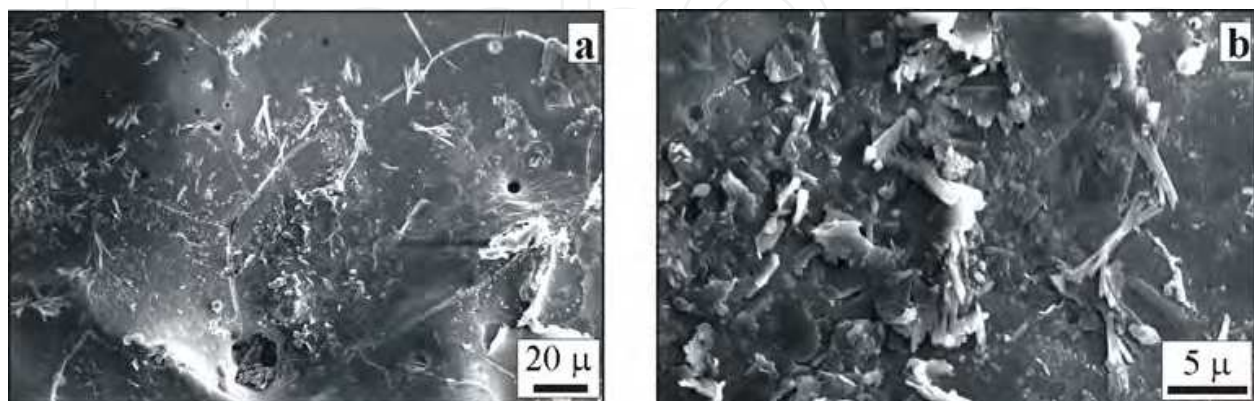


Fig. 13. The microstructure of the fiber tip surface after laser action. **a** - SEM image of a fragment of the fiber end surface; **b** - magnified SEM image of a fragment of the end surface with the crystal-like structures on the surface (Yusupov et al., 2011a).

Typical micron-scale circular holes on the film surface (Fig. 13a) can be caused by cavitation collapse of single bubbles. It is well known that cavitation collapse of bubbles in liquid in the vicinity of the solid surface gives rise to the high-speed cumulative microjets which can destroy the solid surface (Suslick, 1994). Apparently, this effect leads to multiple cracks on the film and the formation of the porous structure (Fig. 13a), since the cumulative microjets can punch holes, cause cracks in the film, and destroy the structure of silica fiber tip.

Collapse of cavitation bubble apart from high pressure generation (up to 10^6 MPa) can cause overheating of gas up to temperatures as high as 10^4 K. Such high values of water pressure and temperature can result in formation of supercritical water (critical pressure of water is $P_c=218$ atm, critical temperature - $T_c=374^\circ\text{C}$), which can dissolve silica fiber (Bagratashvili et al., 2009).

Fig. 14 shows Raman spectra of some areas of laser irradiated fiber tip surface (curves 3-5) compared with that of graphite (1) and diamond (2). Raman bands at 1590 cm^{-1} and 1350 cm^{-1} to diamond and graphite nano-phases correspondingly (Yusupov et al., 2011a).

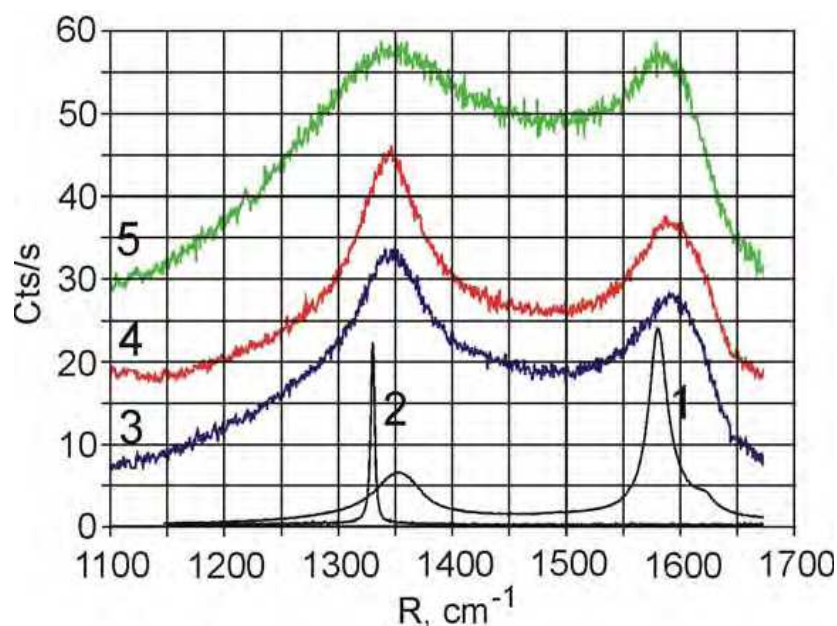
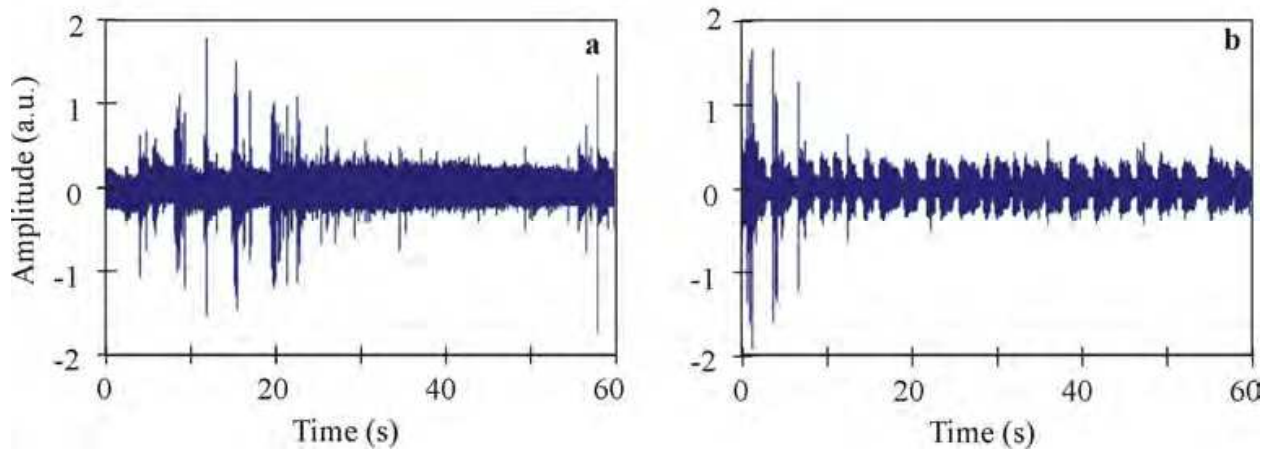


Fig. 14. Raman spectra from different areas of laser fiber tip surface (curves 3, 4 and 5) compared with that of graphite (1) and diamond (2) (Yusupov et al., 2011a).

Formation of diamond nanophase at a fiber tip surface in this case is rationalized by extremely high pressures and temperatures caused by cavitation processes stimulated by laser irradiation (Yusupov et al., 2011a).

5. Laser-induced acoustic effects

Laser-induced hydrodynamics processes in water-saturated bio-tissues causes generation of intense acoustic waves. We have studied the peculiarities of generation of such acoustic waves in water and water-saturated biotissue (intervertebral disc, bone, et al.) in the vicinity of blackened optical fiber tip using acoustic hydrophone (Brul and Kier 8100, Denmark). The hydrophone with 0 - 200 KHz band was placed in water or biotissue at 1cm distance from optical fiber tip. Fig. 15 demonstrates typical example of acoustic response to laser irradiation for two different cases: in the bath of free water (Fig. 15a) and in the case of water

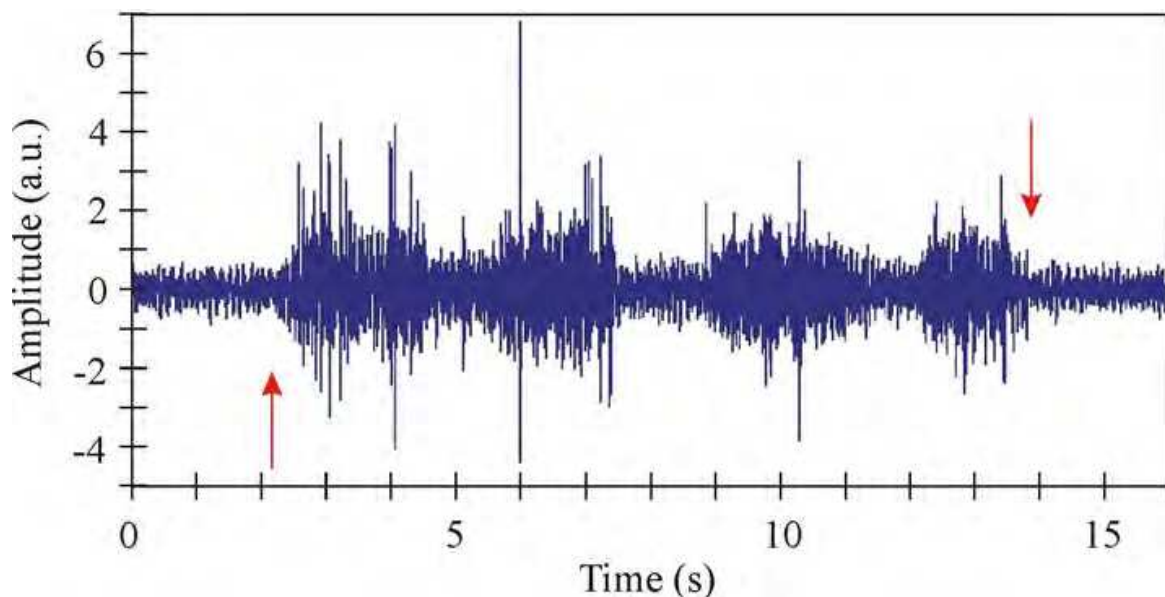


The fiber tip surface is blackened before laser irradiation with $0.97\ \mu\text{m}$ wavelength.

Fig. 15. Fragments of acoustic response to 3 W laser irradiation of water for two different cases: in a bath of free water (a) and in a water-filled capillary (b).

filled capillary (Fig. 15b). In the case of the bath with free water, the short random laser-induced acoustic spikes take place. At the same time, the acoustic response to laser irradiation in the case of water-filled capillary (which imitates situation in real water-filled biotissue channel) is different (Fig. 15b). Acoustic signal is amplitude-modulated by its feature, and low-frequency modulation period is about 2 s.

Fig. 16 demonstrates acoustic response to laser irradiation of nucleus pulposus *in vivo* when optical fiber was moved forward (regime of channels formation in the course of laser healing of degenerated disc). The acoustic signal is non-stationary by its nature. The short-pulse intense acoustic spikes take place and the signal itself is amplitude modulated (similarly to that in water-filled capillary) with a modulation period of about 3 s.



Arrows show the moments of laser on and laser off.

Fig. 16. Acoustic response to 3 W laser irradiation with $0.97\ \mu\text{m}$ wavelength of nucleus pulposus *in vivo*, when optical fiber was moved forward in the intervertebral disc.

The more detailed studies show that for both *in vivo* and *in vitro* cases laser-induced generation of short-pulse intense quasi-periodic acoustic signals. The fragment of spectrogram of acoustic response given at Fig. 17 clearly demonstrates temporal change of spectral components for acoustic signal generated from laser irradiated nucleus pulposus *in vitro* when optical fiber was moved forward in the intervertebral disc (similar to shown at Fig. 1).

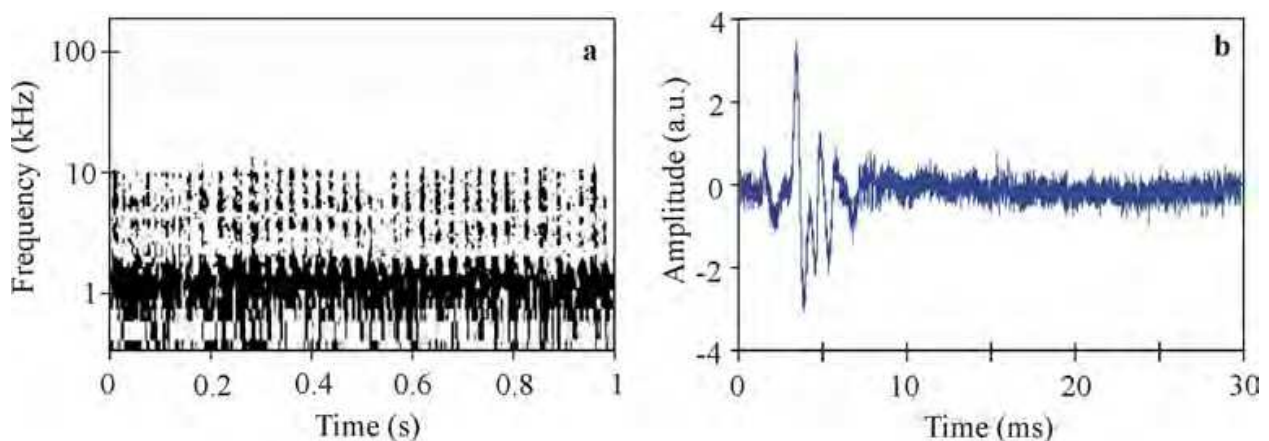


Fig. 17. The fragment of spectrogram (a) and temporal structure of single pulse (b) of acoustic response generated from laser irradiated nucleus pulposus *in vitro*.

As one can see, the acoustic response in this case has the form of short, intense and broadband (from 0 to 10 kHz) pulses of about 10 ms in duration combined into the series of pulses generated with frequency of 40 Hz. Fig. 17b shows that the amplitude of single pulse is an order of amplitude higher than the background acoustic noise. The most of acoustic power is concentrated in such pulses. The broad spectrum of acoustic pulses and their low duration indicate to shock-type of generated acoustic waves. The acoustic noise has broad spectral maxima in the following spectral intervals: 600 – 700 Hz, 1 - 2 kHz and nearby 10 kHz.

Appearance of these bands are caused by the dynamics of vapor-gas mixture and are associated with acoustic resonances of the system. Notice that laser-induced formation of channels in degenerated spinal discs *in vitro* has been accompanied by 4 Hz in frequency strong visual vibrations of needle with laser fiber.

Generation of such a strong acoustic vibrations is caused in our opinion by contact of overheated (up to >1000 °C (Yusupov et al., 2011a)) fiber tip with water and water-saturated tissue of spinal disc. Such contact can result in explosive boiling of water solution nearby the fiber tip and, also, in burning of collagen in cartilage tissues. Intense hydrodynamic processes can take place nearby optical fiber tip, which are caused by fast heating of water and tissue, by generation and collapse of vapor-gas bubbles (Chudnovskii et al., 2010a, 2010b; Leighton, 1994). As a result, the free space of disc or bone is filled by liquid saturated by vapor-gas bubbles. Resonance vibrations are excited, since both disc and bone are quite good acoustic resonators. These vibrations give rise to low-frequency modulation of acoustic noise (Fig. 16) and to quasi-periodic generation of short intense pulses (Fig. 17) (Chudnovskii et al., 2010a). The acousto-mechanic shock-type processes in resonance conditions results in mixing and transport of gas-saturated degenerated tissue in the space of defect (Chudnovskii et al., 2010b). These processes destroy hernia and decrease its density (Fig. 2b), thus lowering the pressure to nervous roots. Another important impact of such processes is the regeneration of disc tissues through the effects of mechanobiology (Buschmann et al., 1995; Bagratashvili et al., 2006).

6. Formation of filaments

In this division we will show that existence of strongly absorbed agents (in a form of Ag nanoparticles, in particular) in laser irradiated water nearby optical fiber tip can result in appearance of filamentary structures of these agents (Yusupov et al., 2011b). Medium power (0.3 – 8.0 W) 0.97 μm in wavelength laser irradiation of water with added Ag nanoparticles (in the form of Ag-albumin complexes) through 400 μm optical fiber stimulates self-organization of filaments of Ag nanoparticles for a few minutes. These filaments represent themselves long (up to 14 cm) liquid gradient fibers with unexpectedly thin (10 – 80 μm) core diameter. They are stable in the course of laser irradiation, being destroyed after laser radiation off. Such effect of filaments of Ag nanoparticles self-organization is rationalized by the peculiarities of laser-induced hydrodynamic processes developed in water in presence of laser light and by formation of liquid fibers.

Fiber laser radiation (LS-0,97 IRE-Polus, Russia) 0-10 W in output and 0.97 μm in wavelength was delivered into water-filled plastic cell through 400 μm transport silica optical fiber, which was placed horizontally in the cell. Low intensity (up to 1 mW) green pilot beam from the built in diode laser was used to highlight the 0.97 μm laser irradiated zone in the cell. The cell was placed at the sample compartment of optical microscope (MC300, MICROS, Austria) equipped with color digital video-camera (Vision). Spectroscopic studies were performed with fiber-optic spectrum analyzer (USB4000, Ocean Optics) and UV/vis absorption spectrometer (Cary 50, Varian). To measure the refraction index of collargol we have applied the fiber-optic reflectometer FOR-11 (LaserChem, Russia), which provides 10^{-4} precision of refraction index measurements at 1256 nm wavelength. Cleavage of transport optical fiber has been always produced just before each experiment. Ten minutes later (to provide reasonable attenuation of hydrodynamic motions in the cell) the drop (0.01–1 ml in volume) of brown colored collargol (complex of 25 nm in size Ag nanoparticles with albumin) has been smoothly introduced into the water cell 0.5-10 mm aside from the optical fiber tip.

Our in situ optical microscopic studies of laser-induced filament formation were accomplished in two different modes: 1) in transmission mode, using illumination with white light from microscope lamp; 2) in scattering mode, using illumination with green light of pilot laser beam through the same transport fiber.

Experiments show that 0.97 μm fiber laser irradiation of water in the cell with introduced collargol drop causes (in some period of time from seconds to minutes) formation of thin and long quite homogenous filaments, growing along the axis of 0.97 μm laser beam in water. These filaments are brown colored (that gives the evidence of enhanced Ag nanoparticles concentration in filament) and can be seen even with unaided eye.

Fig. 18 demonstrates the microscope image (in transmission mode) of one of such filaments. This filament is located along the axis of output laser beam and is about 17 mm in length. The measured profile of optical density of this filament is triangular in its shape with about the same widths along filament (determined at half-maximum) of $\sim 200 \mu\text{m}$.

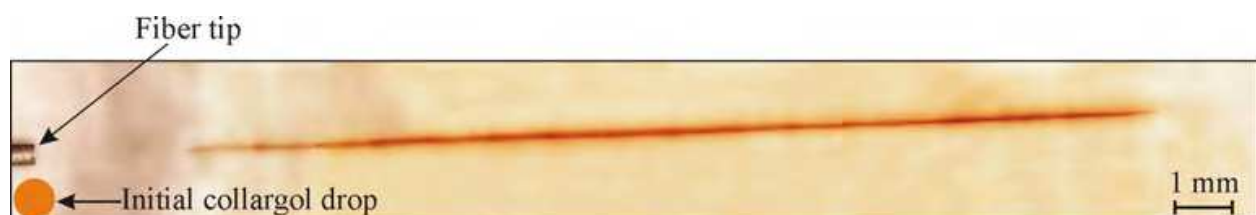


Fig. 18. Micro-image (in transmission mode) of filament of Ag nanoparticles fabricated in water nearby optical fiber tip at 2.5 W of laser power (Yusupov et al, 2011b).

Fig. 19a demonstrates the micro-image of another laser fabricated filament in scattering mode. Intensity of light scattered from this filament decreases gradually with the distance from fiber tip. Attenuation of green light in this case is caused by absorption and scattering of green light in the course of its propagation through the filament. To reveal the peculiarities of filament (given at Fig. 19a) we have performed the following processing of its microscope image: all vertical profiles of image were normalized to local maximum (Fig. 19c); the microscope image was represented in shades of gray (Fig. 19b). As it follows from figures 19b and 19c the length of given filament is about 6 mm, its average width is about 40 μm , and scattering intensity decreases rapidly with the distance from filament axis. Notice that vertical profiles of all fabricated filaments (in both transmission and scattering modes) are almost triangular with a sharp top. It was also established that the end of filament has always a needle-like shape and, also, the width of filament obtained in transmission mode measurements exceeds 3-5 times that obtained in scattering mode.

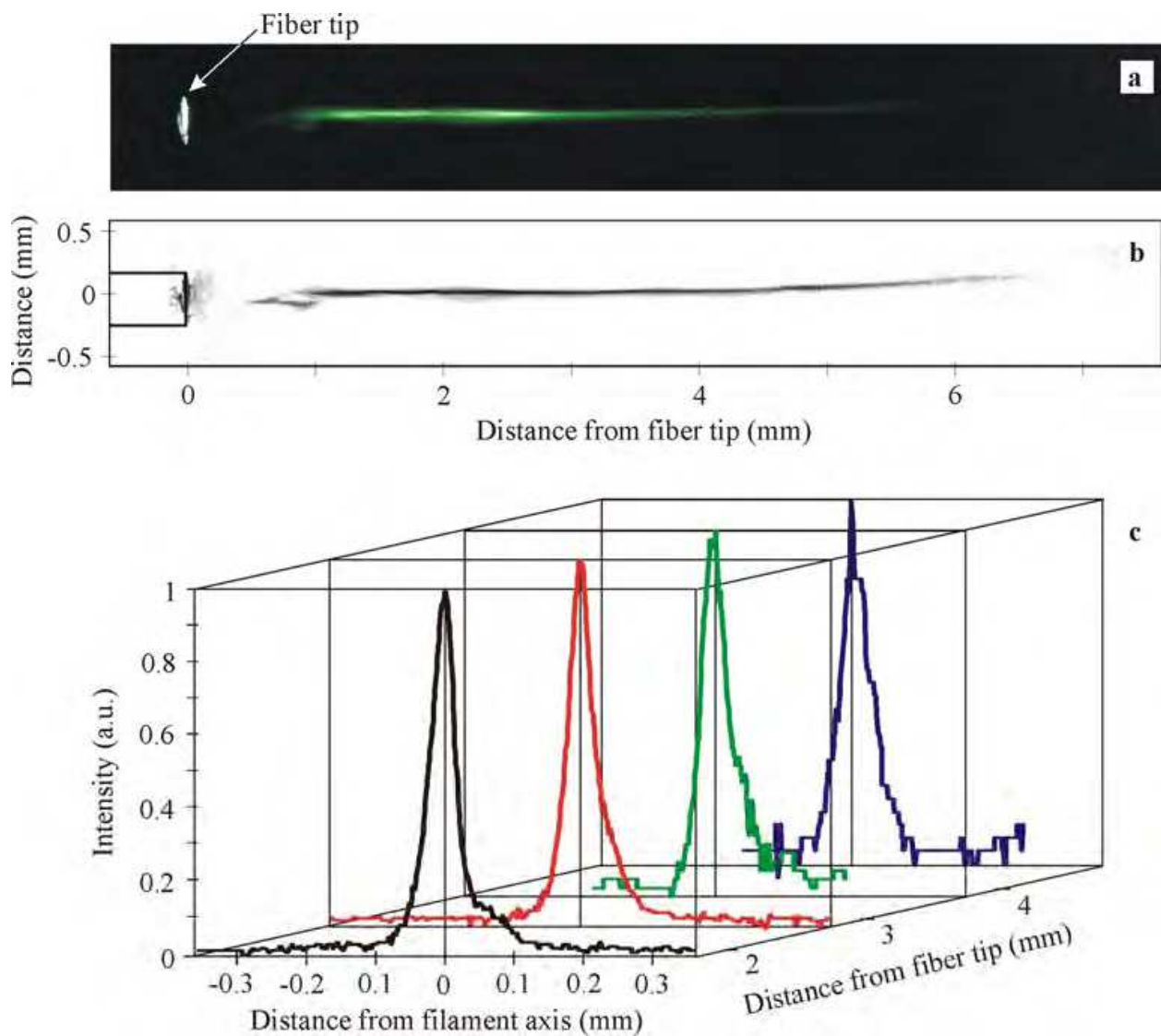


Fig. 19. a - Microscopic picture of filament (in scattering mode) of Ag nanoparticles fabricated in water nearby optical fiber tip at 0.4 W of laser power. b - Image of this filament represented in shades of gray after processing of (see text) of Fig. 19a. c - Normalized vertical profiles of image given at Fig. 19b. (Yusupov et al, 2011b).

It is of importance that filaments of Ag nanoparticles have been formed in our experiments only in the case of existence of initial collargol concentration gradient in laser irradiated water (when collargol drop was introduced initially into water aside from fiber tip). When collargol drop was premixed in water cell before laser irradiation, formation of filaments has never been observed (at any collargol concentrations in the cell and at any laser powers and dozes).

The initial stage of filament self-organization process can be clearly seen in scattering mode (Fig. 4). Some visible hydrodynamic flows take place nearby the fiber tip when laser power is on. Such flows result in intrusion of collargol from neighboring area into the area in front of the fiber tip. The slanting filament structure is clearly seen at Fig. 4. One can also see here the initial process of new intrusion formation (outlined with dashed line). The rate of rise-up front of a given intrusion (which is about 150 μm in average thickness) is found to be described by exponential law (1): at 1 mm from laser fiber tip $V = 1.5 \cdot 10^{-2}$ cm/s, while at 2 mm from laser fiber tip V falls down to $3 \cdot 10^{-3}$ cm/s.

We revealed that filaments of Ag nanoparticles self-organized in the course of 0.97 μm laser irradiation can exist in the cell (in the presence of laser beam and with no external mechanical distortions of liquid in the cell) for quite a long period of time. We have supported such filaments for tens of minutes. Notice that both rectilinear and curved filaments were self-organized in our experiments.

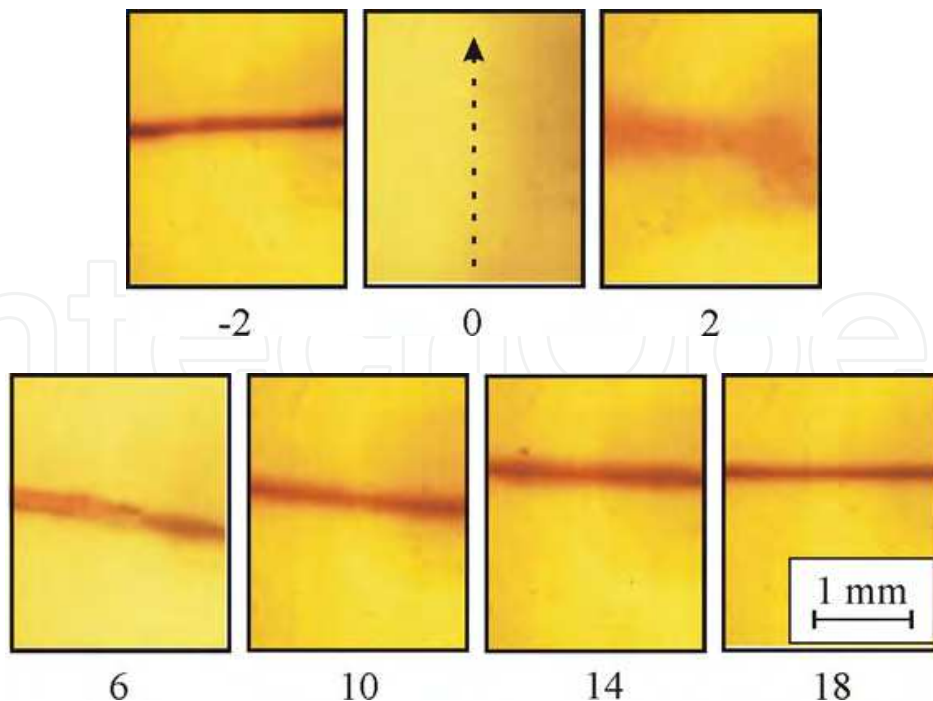
After 0.97 μm laser radiation being off, the filaments of Ag nanoparticles have been completely destroyed for 10 – 30 s period of time. Notice that time Δt of diffusion blooming of filament by value, estimated by formula

$$\frac{-2}{x^2} = D\Delta t = \frac{kT}{3\pi\mu d} \Delta t, \quad (6)$$

where D – is diffusion coefficient of nanoparticle; $k = 1.38 \cdot 10^{-23}$ J/K – Boltzmann constant; $T(K)$ – absolute temperature; $\mu = 1,002 \cdot 10^{-3}$ (N · s/m²) – dynamic viscosity of water; $d = 25$ nm Ag nanoparticle diameter) gives $\Delta t = 25$ s for $x = 100$ μm .

External mechanical distortions of filament of Ag nanoparticles results in its destruction. However after mechanical distortion being off, the filament can be renewed completely in presence of 0.97 μm laser radiation. Fig. 20 shows the dynamic of such filament renovation after the distortion of self-organized filament (produced by its rapid crossing within a metal needle). As one can see from Fig. 20, complete renewal took place for quite a short period of time (~ 20 s).

Our experiments have shown that there is some range of 0.97 μm laser powers for which the effect of laser-induced filament self-organization takes place and is, also, stable and reproducible. At laser powers higher than 8 W we have never observed filament formation. At 0.2-0.5 W laser power filaments have been formed but have been unstable. The most stable and long-living filaments were observed in 0.5-3 W laser power range. At laser power less than 0.2 W we have never observed such filament formation. The instability of filaments and even their absence at high laser powers is caused by intense laser-induced hydrodynamic processes nearby the fiber tip. Our experiments show that the fiber tip surface is gradually covered by a deposit, which absorbs laser radiation quite well. The wide absorption band of deposit observed at fiber tip can be caused by island film of Ag nanoparticles, and, possibly, by elementary carbon absorption (deposited at fiber tip due to albumin thermo-decomposition). As a result of such deposits, the fiber tip becomes an



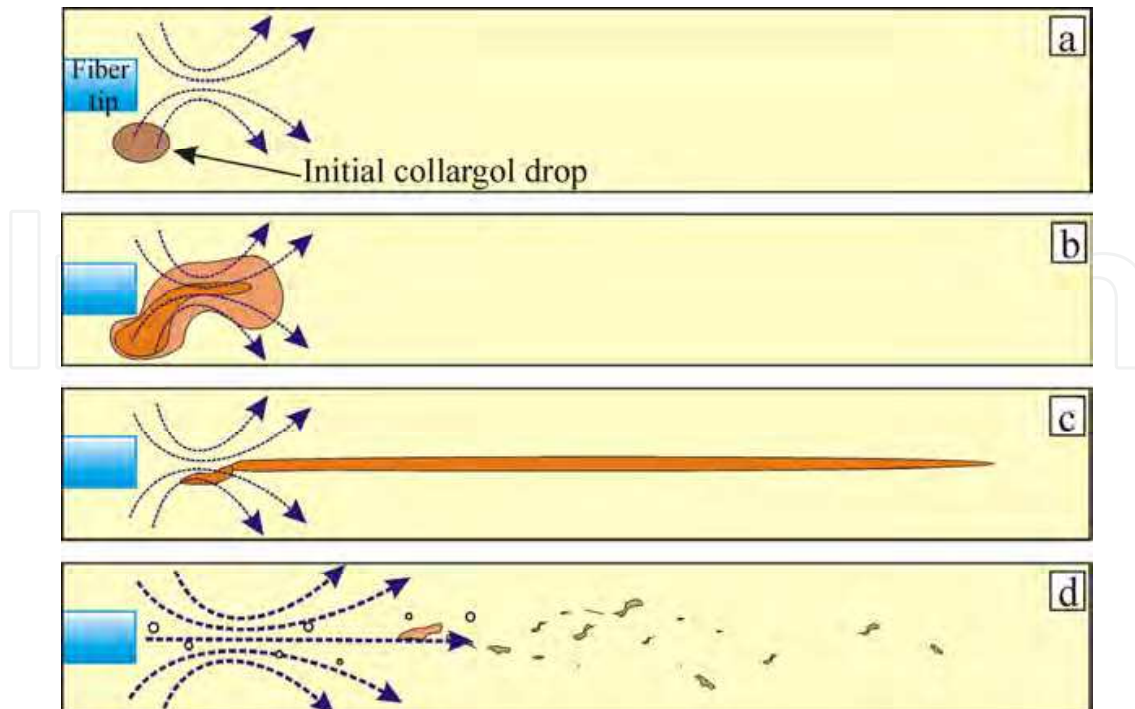
Digits show the period of time from the beginning of filament destruction (Yusupov et al., 2011b).

Fig. 20. Renewal of destroyed filament of Ag nanoparticles in water nearby the tip of optical fiber.

intense heat source. That causes explosive water boiling, intense formation of micro-bubbles, moving rapidly away from fiber tip to liquid (see for example Fig. 1,b) and destroying filament.

We rationalize the observed effect of laser-induced self-organization of filaments from Ag nanoparticles by following mechanisms. Initially (Fig. 21a), laser light absorption by water (the absorption coefficient in water at $0.97 \mu\text{m}$ is about 0.5 cm^{-1}) causes its heating with the $2\text{-}10^\circ\text{C/s}$ rate. Besides, the intense transfer of impulse to water takes place in this case. As a result, the closed axis-symmetric liquid flows are developed being directed from fiber tip. These flows promote Ag nanoparticles intrusion into the laser beam nearby the fiber tip (Fig. 21b). Such intrusions are clearly seen in scattered green laser light (Fig. 4).

Another factor dominates at the second stage of filament self-organization. The refractive index for collargol n_c is higher than that for clean water n_w . The value of $n_c - n_w = 0.0044$ at wavelength $\lambda = 1256 \text{ nm}$ was directly measured in our experiments using fiber-optic densitometer. Due to the effect of total internal reflection laser light is concentrated inside intrusion which work in fact as a liquid optical fiber. Channeling of laser light inside intrusion with Ag nanoparticles results in deeper propagation of laser light into water. Light pressure promotes faster movement of intrusion front giving rise to filament (Fig. 21c). As it was shown in (Brasselet et al., 2008), for example, laser light pressure is also able to force through the boundary between two unmixed liquids and to form thin channel of one liquid inside another one, thus forming liquid optical fiber with gradient core. Thus, the image of filament in transmission mode shows optical density of Ag nanoparticles. At the same time the image of filament in scattering mode clearly demonstrate channeling effect in fabricated filament which in fact is a liquid gradient fiber. Such liquid gradient fiber provides also effective channeling of 970nm laser beam, thus promoting filament elongation and spatial stability.



- Formation of water flow nearby the fiber tip.
- Formation of Ag nanoparticles intrusions.
- Fabrication of filaments from Ag nanoparticles.
- Intense formation of micro-bubbles, hampering filament formation at high laser power.

Fig. 21. To the explanation of the effect of laser-induced formation of filaments of Ag nanoparticles (Yusupov et al., 2011b).

Laser induced formation of 10-50 μm in thickness and up to few millimeters micro-bubble streams (Fig. 11) can also promote the filaments fabrication observed in our experiments. It is clear, however, that too intense chaotic formation of micro-bubble streams observed at high laser power can hamper filament fabrication (Fig. 21d).

We believe that such filaments of nanoparticles can be developed not only in water media but, also, in other fluids, with other laser wavelength and particles types. The indispensable conditions in this case are the availability of sufficient level of laser light absorption in irradiated medium nearby fiber tip and possibility of liquid fiber formation.

7. Conclusion

Hydrodynamic effects induced by a medium power (1-5 W) laser radiation in the vicinity of the heated fiber tip surface in water and in water-saturated tissues are considered. A threshold character of the dynamics of liquid is demonstrated. At a relatively low laser power (about 1 W), the slow formation of vapor-gas bubbles with sizes of hundreds of microns are observed at the optical fiber tip surface. The bubbles can be attached to the tip surface in the course of laser radiation. At higher laser power increases, effective hydrodynamic processes related to the explosive boiling in the vicinity of the overheated fiber tip surface take place. The resulting bubbles with sizes ranging from a few microns to several tens of microns provide the motion of liquid. The estimated velocities of bubbles in

the vicinity of the fiber tip surface can be as high as 100 mm/s. Generation of bubbles in the capillary leads to the circulating water flows with periods ranging from 0.2 to 1 s. Such circulation intensity increases with the laser power. For the laser radiation with a wavelength of 0.97 μm , we observe such effects only for the blackened fiber tip surface, which serves as a local heat source. At a laser power of less than 3 W, stable bubble microjets, which consist of the bubbles (ranging from several to ten microns) can be generated in the vicinity of the blackened tip surface.

Laser-induced hydrodynamic effects in water and bio-tissues can cause the significant degradation of the fiber tip. Cavitation collapse of bubbles in liquid in the vicinity of fiber tip surface gives rise to the high-speed cumulative microjets which can destroy the solid surface. This effect leads to multiple cracks on the film and the formation of the porous structure, formation of supercritical water and even generation of diamonds nano-crystal.

Laser-induced hydrodynamics processes in water and water-saturated bio-tissues are accompanied by generation of intense acoustic waves in resonance conditions, even of shock-type waves. The acousto-mechanic processes results in mixing and transport of gas-saturated degenerated tissue in the space of defect.

We found that medium power (0.3- 8 W) 0.97 μm in wavelength laser irradiation of water with added Ag nanoparticles (in the form of Ag-albumin complexes) through 400 μm optical fiber stimulates self-organization of unexpectedly thin (10-80 μm) and lengthy (up to 14 cm) filaments of Ag nanoparticles in the form of liquid gradient fibers. These filaments in water are stable in the course of laser irradiation being destroyed after laser radiation off. Such effect of filaments of Ag nanoparticles self-organization is rationalized by the peculiarities of laser-induced hydrodynamic processes developed in water in presence of laser light.

8. Acknowledgment

This work is supported by Russian Foundation for Basic Research (grant № 09-02-00714).

9. References

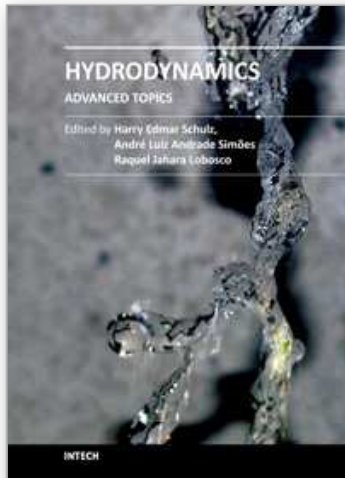
- Bagratashvili V.N., Sobol E.N., Shekhter A.B. (Eds). (2006). *Laser Engineering of Cartilage*. Fizmatlit, ISBN 5-9221-0729-1, Moscow
- Bagratashvili V.N., Konovalov A.N., Novitskiy A.A., Poliakov M., and Tsypina S.I. (2009). Reflectometric studies of the etching of a silica fiber with a germanium silicate core in sub- and supercritical water. *Russian Journal of Physical Chemistry B, Focus on Physics*, Vol. 3, No. 8, pp. 1154-1164, ISSN 1990-7931
- Berry D.W., Heckenberg N.R., and Rubinsztein Dunlop H. (2000). Effects associated with bubble formation in optical trapping. *Journal of Modern Optics*, Vol. 47, No. 9, pp. 1575 – 1585, ISSN 0950-0340
- Brasselet E., Wunenburger R., and Delville J.-P. (2008). Liquid optical fibers with multistable core actuated by light radiation pressure. *Physical Review Letters*, Vol. 101, pp. 1-5, ISSN 1079-7114
- Buschmann M.D., Gluzband Y.A., Grodzinsky A.J., and Hunziker E.B. (1995). Mechanical Compression Modulates Matrix Biosynthesis in Chondrocyte Agarose Culture. *Journal of Cell Science*, Vol. 108, pp. 1497-1508, ISSN 0021-9533

- Chudnovskii V.M. and Yusupov V.I. (2008). Method of Laser Intervention Effects in Osteochondrosis, Patent RF No. 2321373
- Chudnovskii V., Bulanov V., and Yusupov V. (2010a). Laser Induction of Acoustic Hydrodynamical Effects in Medicine. *Photonics*, Vol. 1, pp. 30-36, ISSN 1993-7296
- Chudnovskii V.M., Bulanov V.A., Yusupov V.I., Korskov V.I., and Timoshenko V.S. (2010b). Experimental justification of laser puncture treatment of spine osteochondrosis. *Laser Medicine*, Vol. 14, No. 1, pp. 30-35, ISSN 2071-8004
- Hale G.M. and Querry M.R. (1973). Optical constants of water in the 200-nm to 200- μ m wavelength region. *Applied Optics*, Vol. 12, pp. 555-563, ISSN 0003-6935
- Leighton T. G. (Ed.). (1994). *The Acoustic Bubble*, Academic Press Limited, ISBN 0124419208 9780124419209, London
- Millward-Sadler S.J. and Salter D.M. (2004). Integrin-dependent signal cascades in chondrocyte mechanotransduction. *Annals of Biomedical Engineering*, Vol. 32, No. 3, pp. 435-446, ISSN 0090-6964
- Privalov V.A., Krochek I.V., and Lappa A.V. (2001). Diode laser osteoperforation and its application to osteomyelitis treatment. *Proceedings of the SPIE*, Vol. 4433, pp. 180-185, ISSN 0277-786X
- Rokhsar C.K. and Ciocon D.H. (2009). Fractional Photothermolysis for the Treatment of Postinflammatory Hyperpigmentation after Carbon Dioxide Laser Resurfacing. *Dermatologic Surgery*, Vol. 35, No. 3, (March 2009), pp. 535-537, ISSN 1524-4725
- Sandler B.I., Sulyandziga L.N., Chudnovskii V.M., Yusupov V.I., and Galin Y.M. (2002). *Bulletin physiology and pathology of respiration*, Vol. 11, pp. 46-49, ISSN 1998-5029
- Sandler B.I., Sulyandziga L.N., Chudnovskii V.M., Yusupov V.I., Kosareva O.V., and Timoshenko V.C. (2004). *Prospects for Treatment of Compression Forms of Discogenic Lumbosacral Radiculitis by Means of Puncture Nonendoscopic Laser Operations* (Skoromec A.A.), Dalnauka, ISBN 5-8044-0443-1, Vladivostok
- Suslick K.S. (1994). The chemistry of ultrasound. *The Yearbook of Science & the Future*, pp 138-155, Encyclopaedia Britannica, ISBN 0852294026, Chicago
- Taylor R.S. and Hnatovsky C. (2004). Growth and decay dynamics of a stable microbubble produced at the end of a near-field scanning optical microscopy fiber probe. *Journal of Applied Physics*, Vol. 95, No. 12, (June 2004), pp. 8444-8449, ISSN 0021-8979
- Van den Bos R., Arends L., Kockaert M., Neumann M., Nijsten T. (2009). Endovenous therapies of lower extremity varicosities: a meta-analysis. *Journal of Vascular Surgery*, Vol. 49, No. 1, pp. 230-239, ISSN 0741-5214
- Yusupov V.I., Chudnovskii V.M., and Bagratashvili V.N. (2010). Laser-induced hydrodynamics in water-saturated biotissues. 1. Generation of bubbles in liquid. *Laser Physics*, Vol. 20, No. 7, pp.1641-1646, ISSN 1054 660X
- Yusupov V.I., Chudnovskii V.M., and Bagratashvili V.N. (2011a). Laser-induced hydrodynamics in water-saturated biotissues. 2. Effect on Delivery Fiber. *Laser Physics*, Vol. 21, No. 7, pp. 1230-1234, ISSN 1054 660X

Yusupov V.I., Chudnovskii V.M., Kortunov I.V., Bagratashvili V.N. (2011b). Laser-induced self-organization of filaments from Ag nanoparticles. *Laser Physics Letters*, Vol. 8, No. 3, (March 2011), pp. 214–218, ISSN 1612-2011

IntechOpen

IntechOpen



Hydrodynamics - Advanced Topics

Edited by Prof. Harry Schulz

ISBN 978-953-307-596-9

Hard cover, 442 pages

Publisher InTech

Published online 22, December, 2011

Published in print edition December, 2011

The phenomena related to the flow of fluids are generally complex, and difficult to quantify. New approaches - considering points of view still not explored - may introduce useful tools in the study of Hydrodynamics and the related transport phenomena. The details of the flows and the properties of the fluids must be considered on a very small scale perspective. Consequently, new concepts and tools are generated to better describe the fluids and their properties. This volume presents conclusions about advanced topics of calculated and observed flows. It contains eighteen chapters, organized in five sections: 1) Mathematical Models in Fluid Mechanics, 2) Biological Applications and Biohydrodynamics, 3) Detailed Experimental Analyses of Fluids and Flows, 4) Radiation-, Electro-, Magnetohydrodynamics, and Magnetorheology, 5) Special Topics on Simulations and Experimental Data. These chapters present new points of view about methods and tools used in Hydrodynamics.

How to reference

In order to correctly reference this scholarly work, feel free to copy and paste the following:

V. I. Yusupov, V. M. Chudnovskii and V. N. Bagratashvili (2011). Laser-Induced Hydrodynamics in Water and Biotissues Nearby Optical Fiber Tip, Hydrodynamics - Advanced Topics, Prof. Harry Schulz (Ed.), ISBN: 978-953-307-596-9, InTech, Available from: <http://www.intechopen.com/books/hydrodynamics-advanced-topics/laser-induced-hydrodynamics-in-water-and-biotissues-nearby-optical-fiber-tip>

INTECH
open science | open minds

InTech Europe

University Campus STeP Ri
Slavka Krautzeka 83/A
51000 Rijeka, Croatia
Phone: +385 (51) 770 447
Fax: +385 (51) 686 166
www.intechopen.com

InTech China

Unit 405, Office Block, Hotel Equatorial Shanghai
No.65, Yan An Road (West), Shanghai, 200040, China
中国上海市延安西路65号上海国际贵都大饭店办公楼405单元
Phone: +86-21-62489820
Fax: +86-21-62489821

© 2011 The Author(s). Licensee IntechOpen. This is an open access article distributed under the terms of the [Creative Commons Attribution 3.0 License](#), which permits unrestricted use, distribution, and reproduction in any medium, provided the original work is properly cited.

IntechOpen

IntechOpen